

Electronic Supplementary Information

for

Compact device prototype for turn-on fluorescent detection of Sarin based on reactive 4,4-diaryloxy-BODIPY derivatives

Lu Liu,^{#a} Sheng Li,^{#a} Wendan Luo,^a Jiashuang Yao,^a Taihong Liu,^{*a} Molin Qin,^{*b} Zhiyan Huang,^{*a} Liping Ding^a
and Yu Fang^a

^aKey Laboratory of Applied Surface and Colloid Chemistry of Ministry of Education, School of Chemistry and Chemical Engineering, Shaanxi Normal University, Xi'an 710119, P. R. China

^bState Key Laboratory of NBC Protection for Civilian, Beijing 102205, P. R. China

Corresponding authors: liuth121@snnu.edu.cn (T.L.); qinmolin@139.com (M.Q.); zyhuang@snnu.edu.cn (Z.H.)

[#]L.L. and S.L. contributed equally to this work.

Contents

1. Experimental details	S2
2. Performance comparison of the present method with reported works	S5
3. Single crystal analysis	S6
4. Supplementary figures and tables	S8
5. Sensing mechanism analysis	S11
6. Detection performances of the compact device prototype	S12
7. NMR spectra of the spiranic 4,4-diaryloxy-BODIPY fluorophores	S13
8. HRMS spectra of the spiranic 4,4-diaryloxy-BODIPY fluorophores	S16
References	S18

1. Experimental details

1.1. Materials and characterization methods

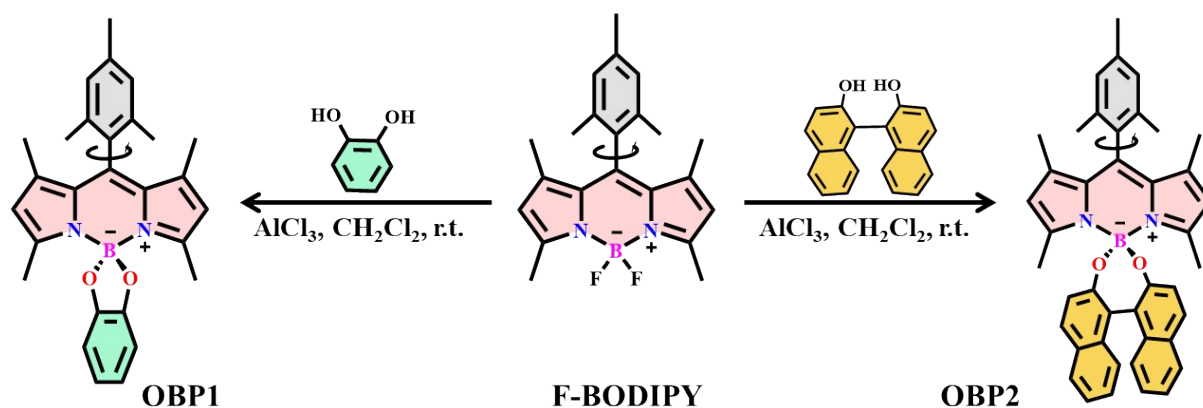
Acetonitrile (ACN), tetrahydrofuran (THF), acetone (ACE), dichloromethane (DCM), benzene (BEN), toluene (TOL), *n*-hexane (HEX) and other reagents were commercially available without further purification unless otherwise noted. Thin-layer chromatography (TLC) was performed on precoated silica gel 60 F254 plates. Column chromatography was performed over silica gel 230-400 mesh. NMR (^1H , ^{13}C , and ^{11}B) measurements were performed at room temperature using a Bruker AVANCE^{III} NMR spectrometer with tetramethylsilane (TMS) as an internal reference. High-resolution mass spectra (HRMS) were acquired in atmospheric pressure chemical ionization (APCI) sources using a Bruker maxis UHR-TOF mass spectrometer. MALDI-TOF MS analysis was performed on the Bruker Autoflex mass spectrometer. The optical properties of the spiranic 4,4-diaryloxy-BODIPY fluorophores were investigated in the spectroscopic-grade solvents. UV-vis spectra were recorded using a Hitachi U-3900/3900H spectrometer in 10 mm path length quartz cuvettes. Steady-state fluorescence emission spectra were obtained using a fluorescence spectrometer (Edinburgh FLS980) with a xenon lamp as the light source at room temperature. The absolute fluorescence quantum yields (Φ_{F}) were obtained using a Hamamatsu C9920-02G instrument with a Xe excitation source and a Hamamatsu A10080-01 monochromator.

1.2. Synthesis details of the spiranic 4,4-diaryloxy-BODIPY derivatives

Two spiranic 4,4-diaryloxy-BODIPY derivatives denoted as **OBP1** and **OBP2** were synthesized through a one-step strategy starting from the corresponding parent 4,4-difluoro-BODIPY and purified according to the reported procedures.¹⁻⁵

General synthesis of the spiranic 4,4-diaryloxy-BODIPY derivatives: Under N_2 atmosphere, a mixture of 1,3,5,7-tetramethyl-8-(2',4',6'-trimethylbenzene)-4,4-difluoro-BODIPY (F-BODIPY, 366.0 mg, 1.0 mmol) and aluminium chloride (AlCl_3 , 332.5 mg, 2.5 mmol) in dry CH_2Cl_2 (30 mL) was stirred for 5 min at 40°C . The reaction was monitored by TLC method until the raw material consumed up. After cooling down to room temperature, the solid of 1,2-benzene-diol or 1,1'-

binaphth-2,2'-diol was added properly. The resultant mixture was stirred at room temperature for another 30 min. Then the organic mixture was washed twice with water (10 mL × 2) and dried over anhydrous Na₂SO₄. The organic solvent was removed by evaporating under reduced pressure, and the resultant residue was purified by column chromatography.



Scheme S1. General synthesis procedure for compounds **OBP1** and **OBP2**.

Compound OBP1: As aforementioned, F-BODIPY (366.0 mg, 1.0 mmol) was reacted with 1,2-benzene-diol (275.0 mg, 2.5 mmol). The resultant residue was purified by column chromatography (*n*-pentane/CH₂Cl₂ = 5/1, then 2/1) to obtain compound **OBP1** (423 mg, yield ~ 97%) as an orange solid. ¹H NMR (400 MHz, CDCl₃, ppm): δ 6.96 (s, 2H), 6.82 - 6.76 (m, 4H), 5.93 (s, 2H), 2.34 (s, 3H), 2.13 (s, 6H), 2.08 (s, 6H), 1.38 (s, 6H). ¹³C NMR (100 MHz, CDCl₃, ppm): δ 157.1, 151.8, 142.9, 141.7, 138.7, 135.0, 131.4, 131.3, 129.1, 122.0, 119.6, 108.8, 21.3, 19.6, 15.3, 13.7. ¹¹B NMR (128 MHz, CDCl₃, ppm): δ 6.14 (s, 1B). HRMS (APCI), *m/z*, [M+H]⁺: calculated for C₂₈H₃₀BN₂O₂⁺: 437.2400, found: 437.2403.

Compound OBP2: As aforementioned, F-BODIPY (366.0 mg, 1.0 mmol) was reacted with 1,1'-binaphthyl-2,2'-diol (1.43 g, 5.0 mmol). The resultant residue was purified by column chromatography (*n*-pentane/CH₂Cl₂ = 5/1, then 2/1) to obtain compound **OBP2** (533 mg, yield ~ 87%) as an orange-reddish solid. ¹H NMR (400 MHz, CDCl₃, ppm): δ 7.82 - 7.80 (d, *J* = 8.2 Hz, 2H), 7.76 - 7.73 (d, *J* = 8.8 Hz, 2H), 7.31 - 7.21 (d, *J* = 7.5 Hz, 2H), 7.19 (d, *J* = 8.5 Hz, 2H), 7.14 - 7.10 (m, 4H), 6.97 (s, 2H), 5.74 (s, 2H), 2.35 (s, 3H), 2.21 (s, 6H), 1.73 (s, 6H), 1.38 (s, 6H). ¹³C NMR (100 MHz, CDCl₃, ppm): δ 156.1, 154.3, 142.2, 141.5, 138.6, 135.3, 133.9, 131.9, 131.7,

130.0, 129.2, 129.1, 127.9, 127.3, 125.3, 124.0, 123.4, 121.8, 121.4, 21.4, 19.7, 16.3, 13.8. ^{11}B NMR (128 MHz, CDCl_3 , ppm): δ 3.53 (s, 1B). HRMS (APCI), m/z , $[\text{M}+\text{H}]^+$: calculated for $\text{C}_{42}\text{H}_{38}\text{BN}_2\text{O}_2^+$: 613.3028, found: 613.3032.

1.3. X-ray single crystal of compound **OBP1**

The single crystal of compound **OBP1** was grown from the $\text{CH}_2\text{Cl}_2/n$ -hexane solution following the slow diffusion strategy. All data were obtained using a Bruker APEX II CCD detector/D8 diffractometer using Cu (Ga, Mo) $K\alpha$ radiation. The data were corrected for absorption through Gaussian integration from indexing of the crystal faces. Structures were solved and refinements were completed using the program using the SHELXL-97. Details of cell data, lengths, angles and refinement data of compound **OBP1** as an example were summarized in Table S2.

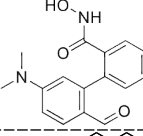
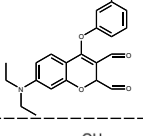
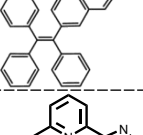
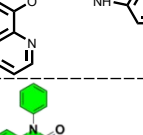

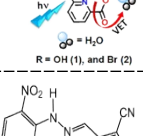
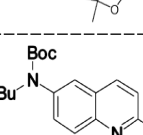
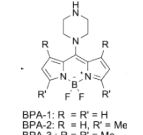
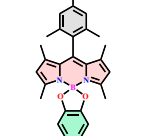
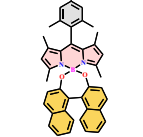
1.4. G-series simulants and real samples

G-series simulants including diethylchlorophosphate (DCP) and diethyl cyanophosphonate (DCNP) with less toxicity were obtained commercially. For safety reasons, they were used firstly to investigate and understand the chemical reactivity of the certain functional groups of the chemical warfare agents (CWAs). Detection limits (DLs) of compounds **OBP1** and **OBP2** to DCP and DCNP were determined based on the fluorescence titration method.⁶⁻⁸ Tabun (GA), Sarin (GB), Soman (GD), and Cyclosarin (GF) are generally real G-series nerve agents. The interferences like triethyl phosphate (TEP), tributyl phosphonate (TBP), diethyl methylphosphonate (DEMP), and dimethyl methylphosphonate (DMMP) were of analytical grade and used as received.

Safety Caution: Only highly qualified and experienced personnel could handle the CWAs. The tests of G-series nerve agents conducted in the present work were carried out in the State Key Laboratory of NBC Protection for Civilian, Institute of Chemical Defense. Due to the high volatility of G-series nerve agents, all experiments were carried out inside safety fume-hoods, operating under efficient filtro-ventilation systems. To avoid any risk of CWA inhalation, respiratory protection of involved personnel was provided by protective breathing masks equipped with combined NBC filters.

2. Performance comparison of the present methods with reported works

Table S1. Performance comparison of the reported methods with present work for detecting DCP.

No.	Compound	Signal	Sensing Techniques	Sample State	DL	References
#1		fluorescence turn-on	paper strip	solution	10.4 nM	<i>Anal. Chem.</i> 2019 , <i>91</i> , 10979
#2		fluorescence turn-on	strip test soil test bio imaging	solution	6.9 nM	<i>ACS Appl. Bio. Mater.</i> 2021 , <i>4</i> , 7007
#3		fluorescence turn-on	---	solution	40 μM	<i>J. Mater. Chem. C</i> 2023 , <i>11</i> , 4025
#4		fluorescence weak-on	dip-stick	solution	10 nM	<i>Anal. Methods</i> 2023 , <i>15</i> , 6417
#5		fluorescence turn-on	test strip	solution	4.7 nM	<i>ACS Sens.</i> 2023 , <i>8</i> , 1220
#6		fluorescence turn-on	---	solution	---	<i>ACS Sens.</i> 2020 , <i>5</i> , 1268
#7		colorimetric Sensing	paper strip	film	25 ppm	<i>ACS Omega</i> 2022 , <i>7</i> , 5595
#8		fluorescence -response	test strip	solution	8 nM	<i>ACS Sens.</i> 2017 , <i>2</i> , 834
#9		fluorescence turn-on	test strip	solution	15 nM	<i>Dyes Pigm.</i> 2021 , <i>189</i> , 109257
#10		fluorescence turn-on	compact device	solution	13.2 nM 8.2 nM	Present Work

3. Single crystal analysis of compound OBP1

The crystallographic information about OBP1 has been deposited to Cambridge Crystallographic Data Centre and signed as CCDC code 2367202. Two OBP1 molecules present in per unit cell indicated the triclinic crystal system. The trimethylbenzene unit at 8-position nearly oriented perpendicular to the BODIPY core with a dihedral angle of 83.9° due to the steric hindrance. While a typical tetrahedral geometry around the boron atom was obtained in OBP1, and a large dihedral angle of 123.0° for 1,2-benzenediol substituent was found. The resultant less π -conjugation implied little conjugation effect on the spectroscopic properties of the spiranic 4,4-diaryloxy-BODIPYs.

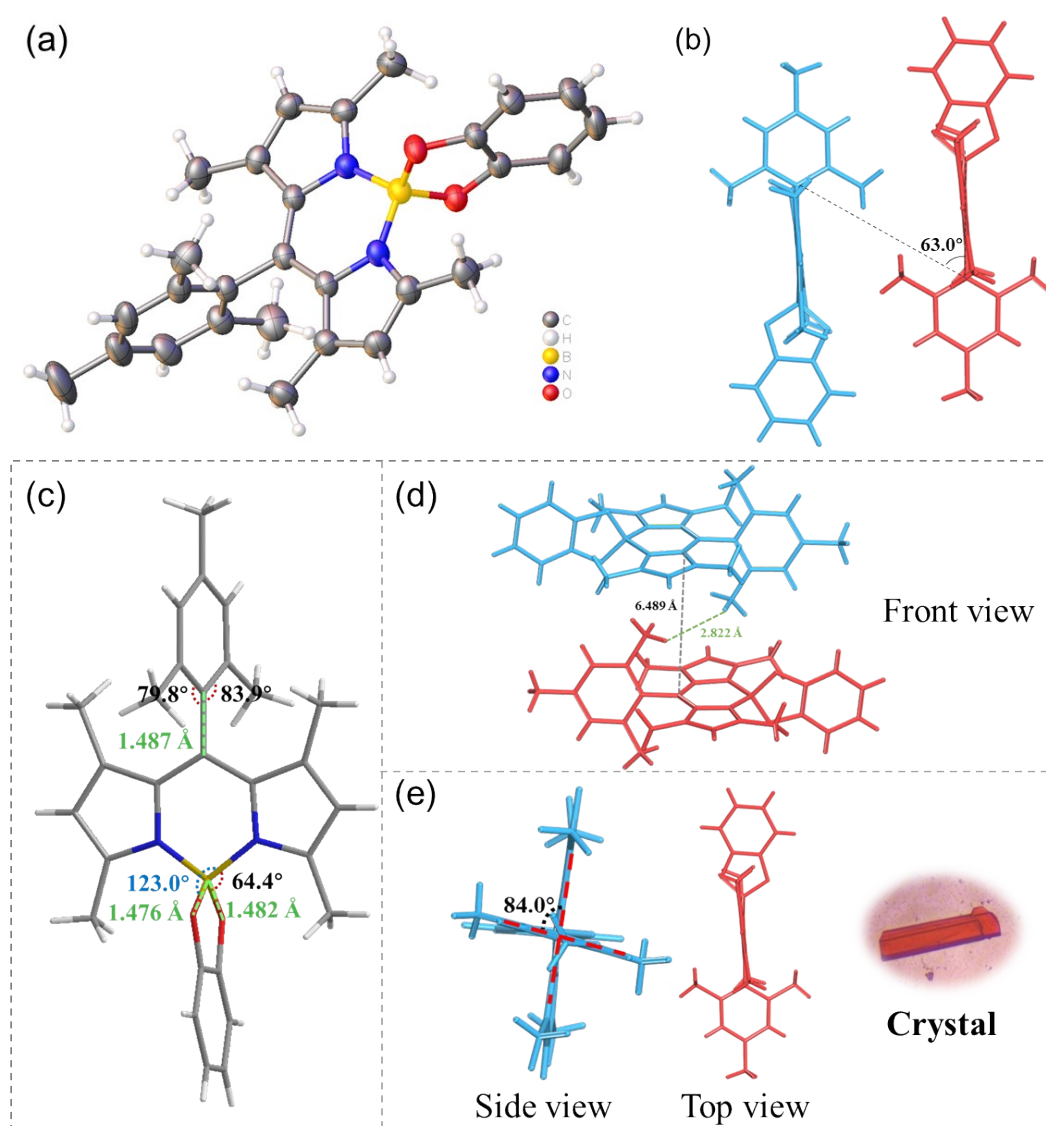


Figure S1. Different crystal conformers (a, b, c) of compound OBP1 obtained from the single crystal X-ray structure analysis. (d) Packing mode of compound OBP1. (e) Crystal packing structure of OBP1 from side view.

Table S2. Crystallographic data and structure refinement of compound **OBP1** obtained from CH₂Cl₂/*n*-hexane.

Compound	OBP1
CCDC	2367202
Empirical formula	C ₂₈ H ₂₉ BN ₂ O ₂
Formula weight	436.34
Temperature/K	268
Crystal system	Triclinic
Space group	<i>P</i> -1
<i>a</i> / Å	7.7983(4)
<i>b</i> / Å	11.6527(7)
<i>c</i> / Å	13.2826(8)
α / °	77.243(3)
β / °	87.408(2)
γ / °	86.971(2)
Volume / Å ³	1174.87(12)
<i>Z</i>	2
Density (calculated) g/cm ³	1.233
μ / mm ⁻¹	0.077
<i>F</i> (000)	464
Crystal size/mm ³	0.3 × 0.2 × 0.1
Radiation	MoK α (λ = 0.71073)
2 θ range for data collection/°	4.944 to 107.828
Index ranges	-9 ≤ <i>h</i> ≤ 9, -14 ≤ <i>k</i> ≤ 14, -16 ≤ <i>l</i> ≤ 16
Reflections collected	31875
Independent reflections	4825 [<i>R</i> _{int} = 0.0600, <i>R</i> _{sigma} = 0.0377]
Data/restraints/parameters	4825/0/305
Goodness-of-fit on <i>F</i> ²	1.069
Final <i>R</i> indexes [<i>I</i> >= 2 σ (<i>I</i>)]	<i>R</i> ₁ = 0.0456, <i>wR</i> ₂ = 0.1233
Final <i>R</i> indexes [all data]	<i>R</i> ₁ = 0.0627, <i>wR</i> ₂ = 0.1412
Largest diff. peak/hole/e Å ⁻³	0.34 / -0.33

4. Supplementary figures and tables

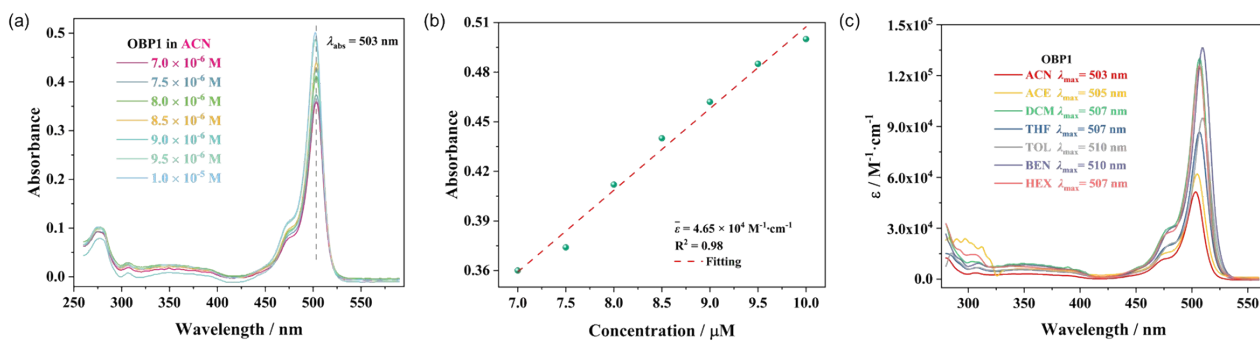


Figure S2. (a) UV-vis absorption spectra of compound **OBP1** in ACN at different concentrations. (b) Corresponding linear relationship of the absorbance intensities with the concentrations of **OBP1**. (c) UV-vis absorption spectra of **OBP1** in kinds of solvents including ACN, THF, ACE, DCM, BEN, TOL, and HEX ($\lambda_{\text{ex}} = 460 \text{ nm}$, $c \sim 8.0 \times 10^{-6} \text{ M}$).

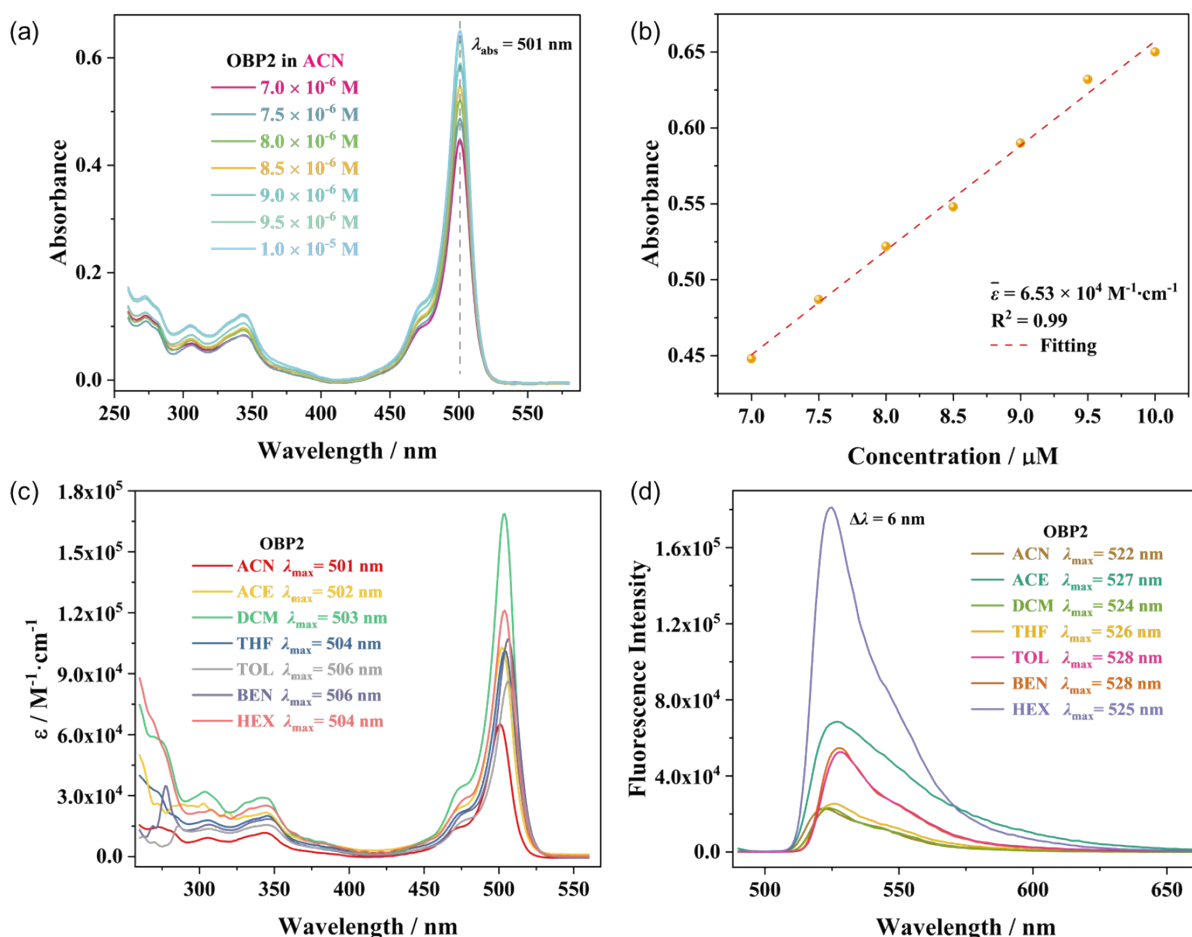


Figure S3. (a) UV-vis absorption spectra of compound **OBP2** in ACN at different concentrations. (b) Corresponding linear relationship of the absorbance intensities with the concentrations of **OBP2**. UV-vis absorption spectra (c, $c_{\text{OBP2}} \sim 8.0 \times 10^{-6} \text{ M}$) and fluorescence emission spectra (d, $\lambda_{\text{ex}} = 460 \text{ nm}$, $c_{\text{OBP2}} \sim 8.0 \times 10^{-5} \text{ M}$) of **OBP2** in kinds of solvents including ACN, THF, ACE, DCM, BEN, TOL, and HEX.

Table S3. Summarized optical properties of compounds **OBP1** and **OBP2** for the $\pi \rightarrow \pi^*$ transition.

Solv.	Δf	OBP1			OBP2				
		$\lambda_{\text{abs}} / \text{nm}$	$\varepsilon / \text{M}^{-1}\cdot\text{cm}^{-1}$	fwhm / nm	$\lambda_{\text{abs}} / \text{nm}$	$\varepsilon / \text{M}^{-1}\cdot\text{cm}^{-1}$	fwhm / nm	$\lambda_{\text{em}} / \text{nm}$	$\Delta\lambda / \text{nm}$
ACN	0.305	503	4.65×10^4	18	501	6.53×10^4	19	522	21
ACE	0.284	505	6.20×10^4	18	502	1.03×10^5	18	527	25
DCM	0.228	507	1.30×10^5	18	503	1.69×10^5	17	524	21
THF	0.208	507	8.68×10^4	18	504	1.02×10^5	19	526	22
TOL	0.015	510	9.49×10^4	18	506	8.63×10^4	18	528	22
BEN	0.0016	510	1.36×10^5	19	506	1.07×10^5	18	528	22
HEX	0.0013	507	1.26×10^5	18	504	1.21×10^5	18	525	21

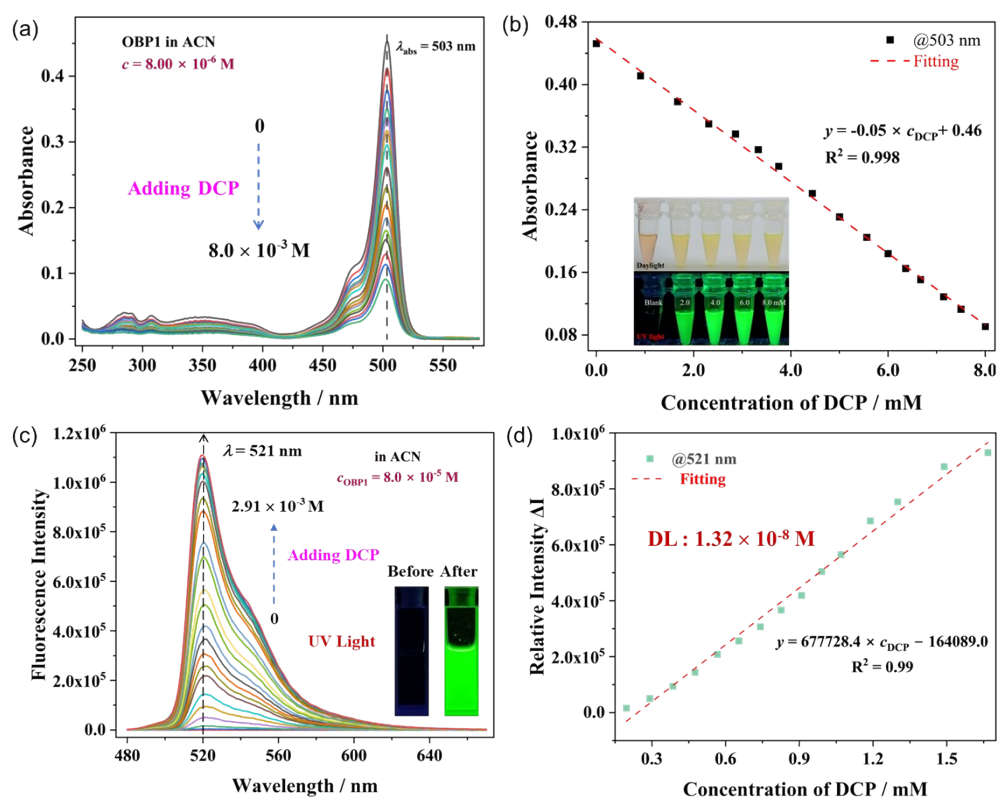


Figure S4. (a) Concentration-dependent UV-vis absorption spectra of OBP1 ($c \sim 8.0 \times 10^{-6} \text{ mol/L}$) with increasing DCP in ACN. (b) Corresponding linear relationship between the absorbance intensity at 503 nm ($A_{503 \text{ nm}}$) of compound **OBP1** and the concentration of the simulant DCP. Inset showed the fluorescence color changes at the different concentrations of DCP in ACN. (c) Fluorescence emission spectra of **OBP1** in ACN upon the gradual addition of DCP ($c = 0 \sim 3.0 \text{ mM}$). Inset showed the fluorescence color changes in the absence and presence of DCP in ACN. (d) Plot of fluorescence emission intensity changes ($\Delta I = I - I_0$) of **OBP1** at 521 nm with the concentrations of DCP in ACN. *Notes:* instrument slide = 0.5, Xe light source, power = 400 W.

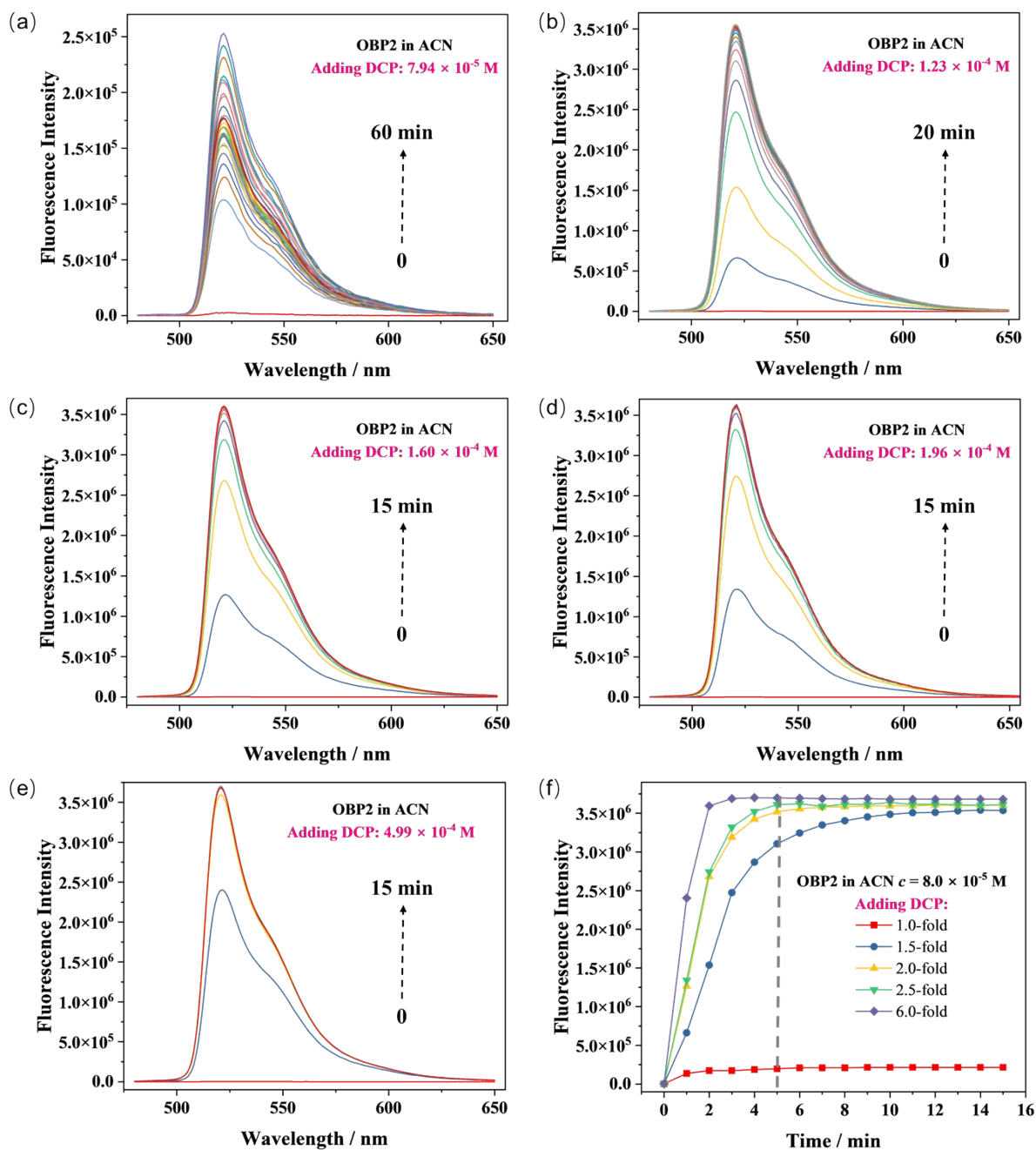


Figure S5. Fluorescence emission spectra of **OBP1** in ACN upon the different reaction time of the simulant DCP (a-e) ($c_{\text{DCP}} \sim 8.0 \times 10^{-5}$ M). (f) Plot of fluorescence emission intensity of **OBP1** at 521 nm with the different concentrations of DCP under different reaction time in ACN. *Notes:* instrument slide = 0.7, Xe light source, power = 400 W.

5. Sensing mechanism analysis

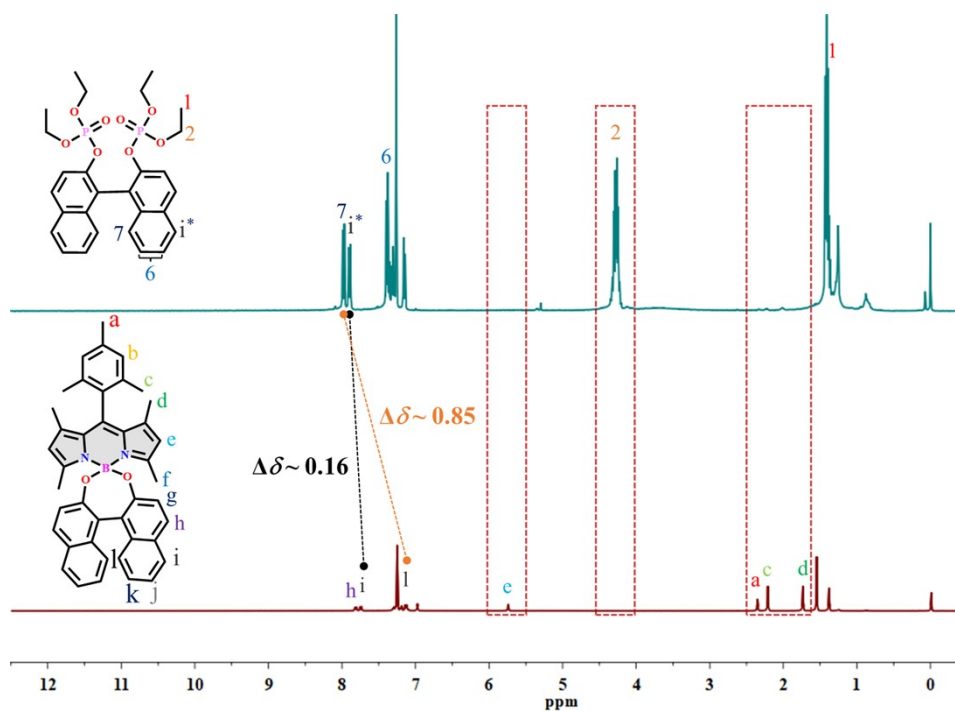


Figure S6. Partial ^1H NMR spectral changes and chemical shifts of compound **OBP2** and the leaving group, 1,1'-binaphthalene-2,2'-diyltetraethyl bis(phosphate), in CDCl_3 (298K).

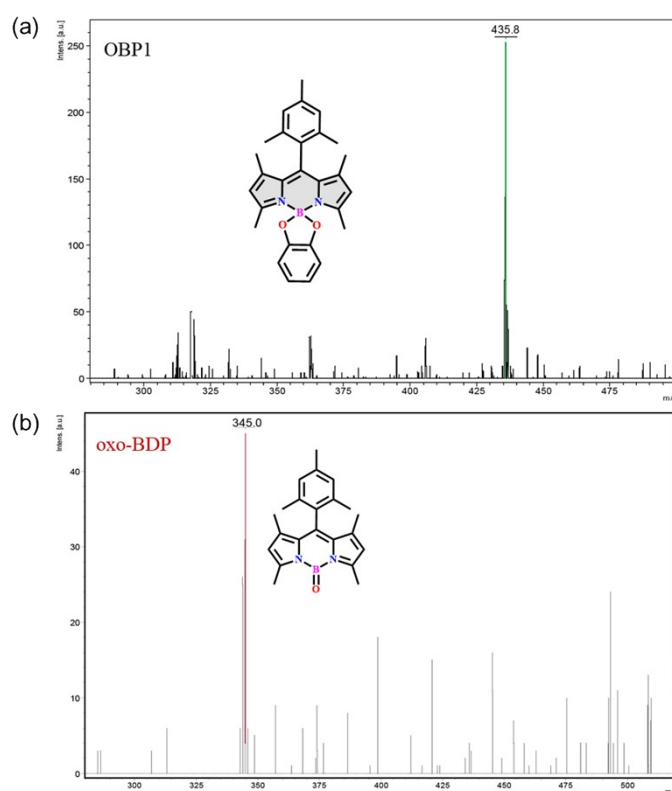


Figure S7. (a) MALDI-TOF spectrum of compound **OBP1** ($[\text{M}-\text{H}]^-$, $\text{C}_{28}\text{H}_{28}\text{BN}_2\text{O}_2^-$, theoretical MW 435.4, found 435.8). (b) MALDI-TOF spectrum of the plausible generated oxo-BDP, 4-(oxo)borane-1,3,5,7-tetramethyl-8-(2',4',6'-trimethylbenzene) ($[\text{M}+\text{H}]^+$, $\text{C}_{22}\text{H}_{26}\text{BN}_2\text{O}^+$, theoretical MW 345.2, found 345.0).

6. Detection performances of the compact device prototype

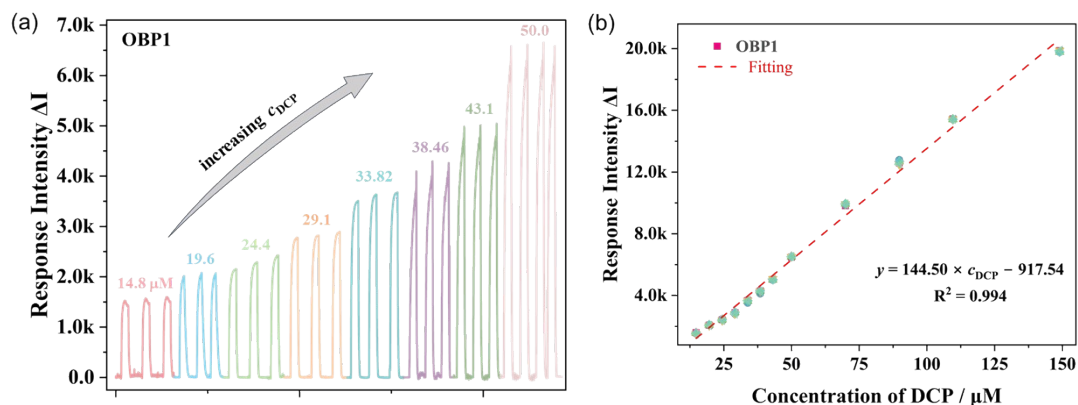


Figure S8. (a) Responses traces of compound **OBPI** to the simulat DCP in ACN using the home-made compact device. (b) Relevant linear relationship of the response intensity of **OBPI** to DCP. *Notes:* Each test was repeated at least three times.

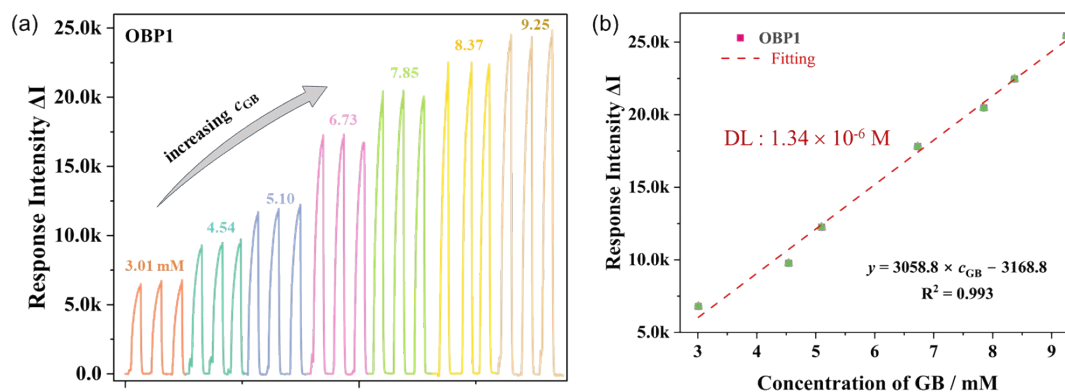


Figure S9. (a) Responses traces of compound **OBPI** to the real Sarin (GB) sample in ACN using the home-made compact device. (b) Relevant linear relationship of the response intensity of **OBPI** to different concentrations of GB. *Notes:* Each test was repeated at least three times.

7. NMR spectra of the spiranic 4,4-diaryloxy-BODIPY fluorophores

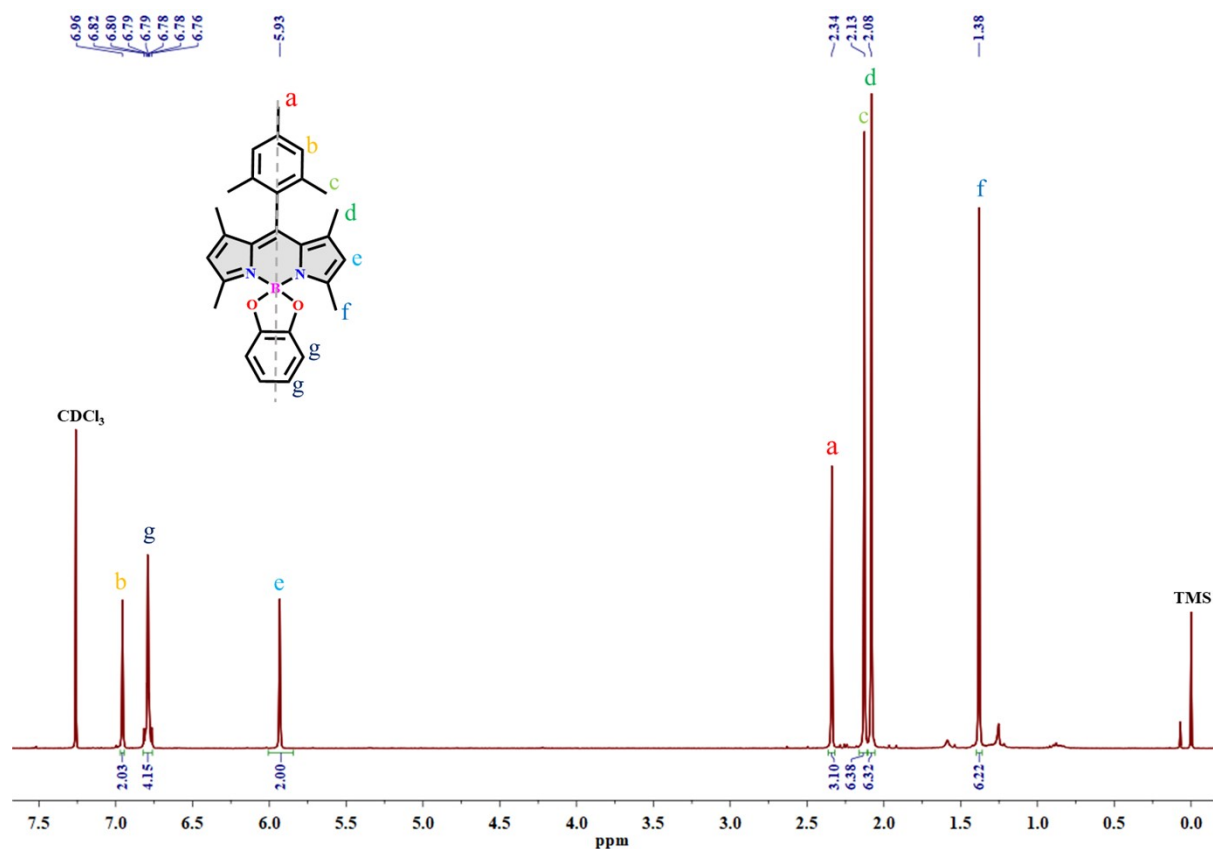


Figure S10. ¹H NMR spectrum of compound **OBPI** in CDCl₃ (298 K).

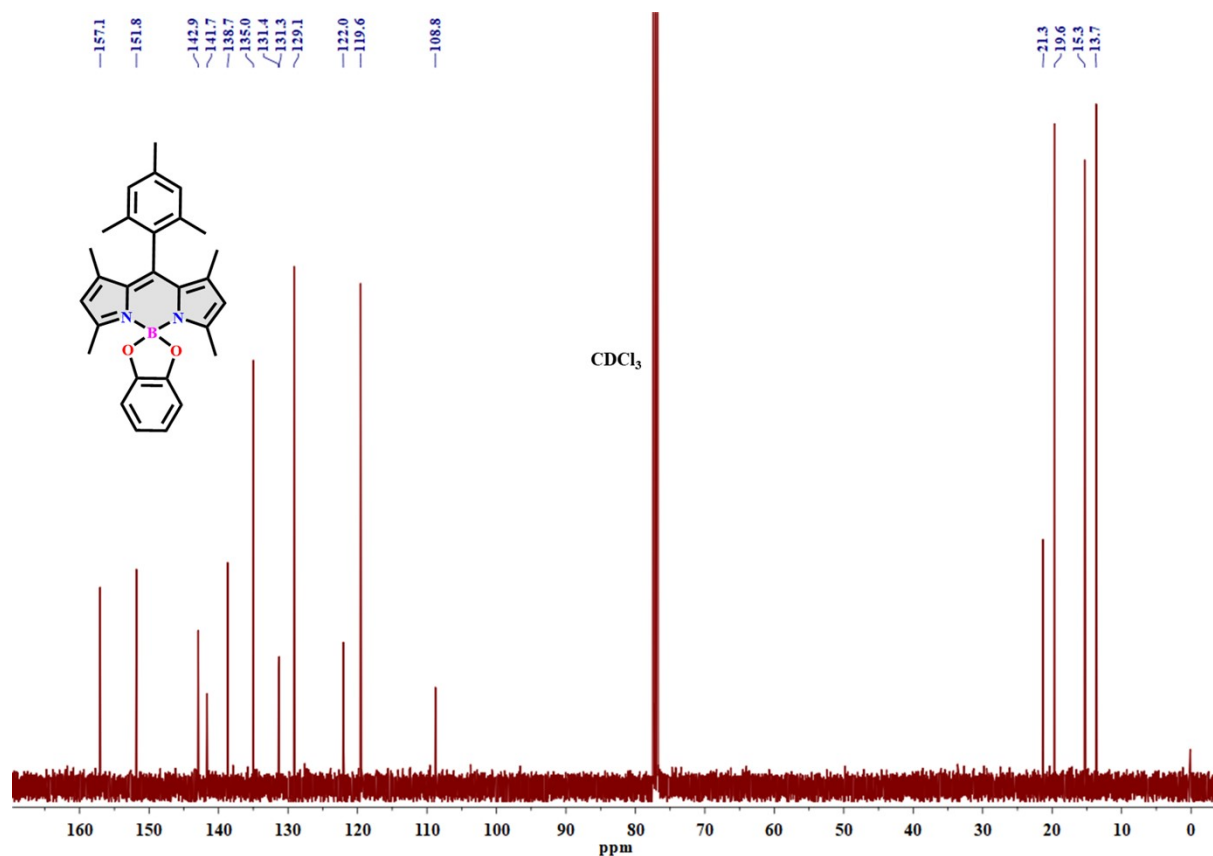


Figure S11. ¹³C NMR spectrum of compound **OBPI** in CDCl₃ (298 K).

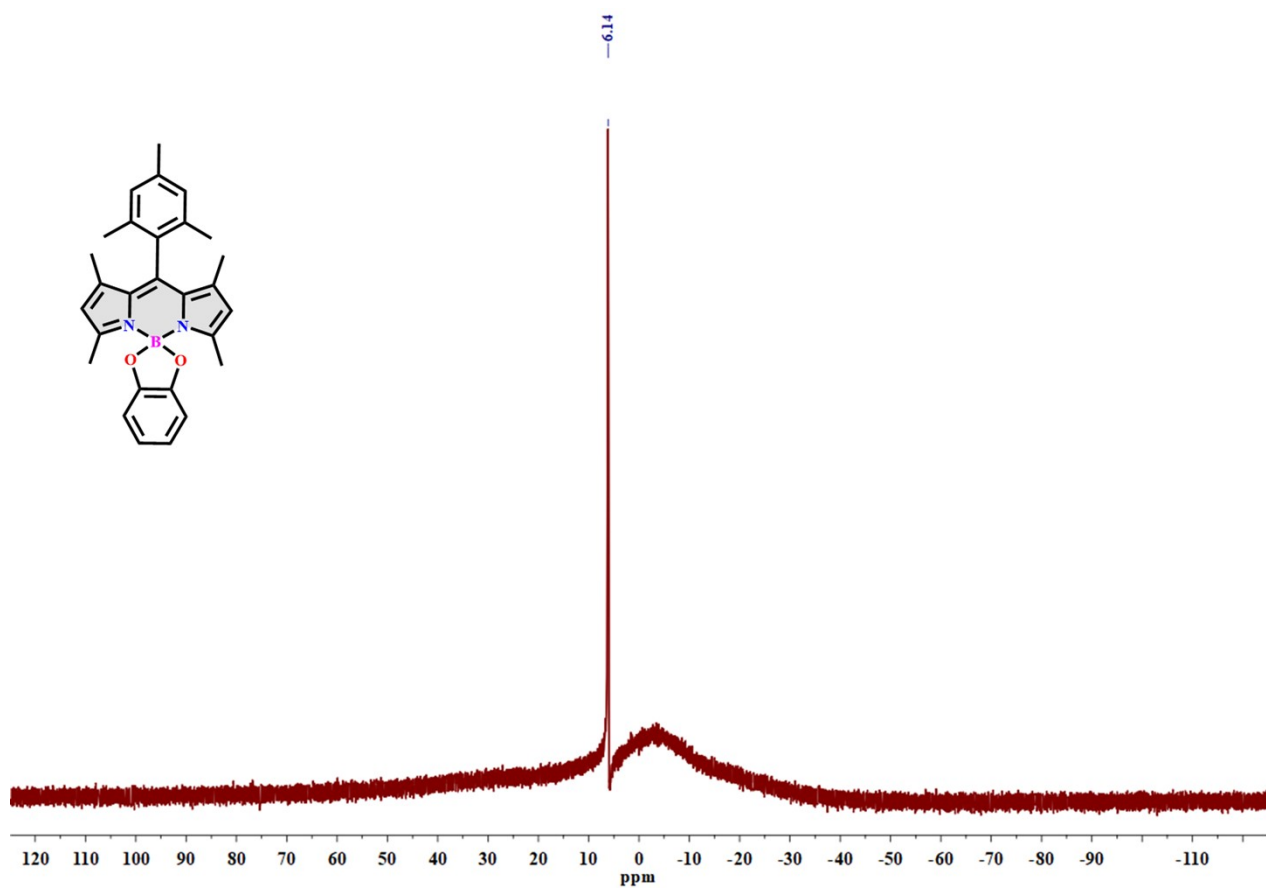


Figure S12. ^{11}B NMR spectrum of compound **OBP1** in CDCl_3 (298 K).

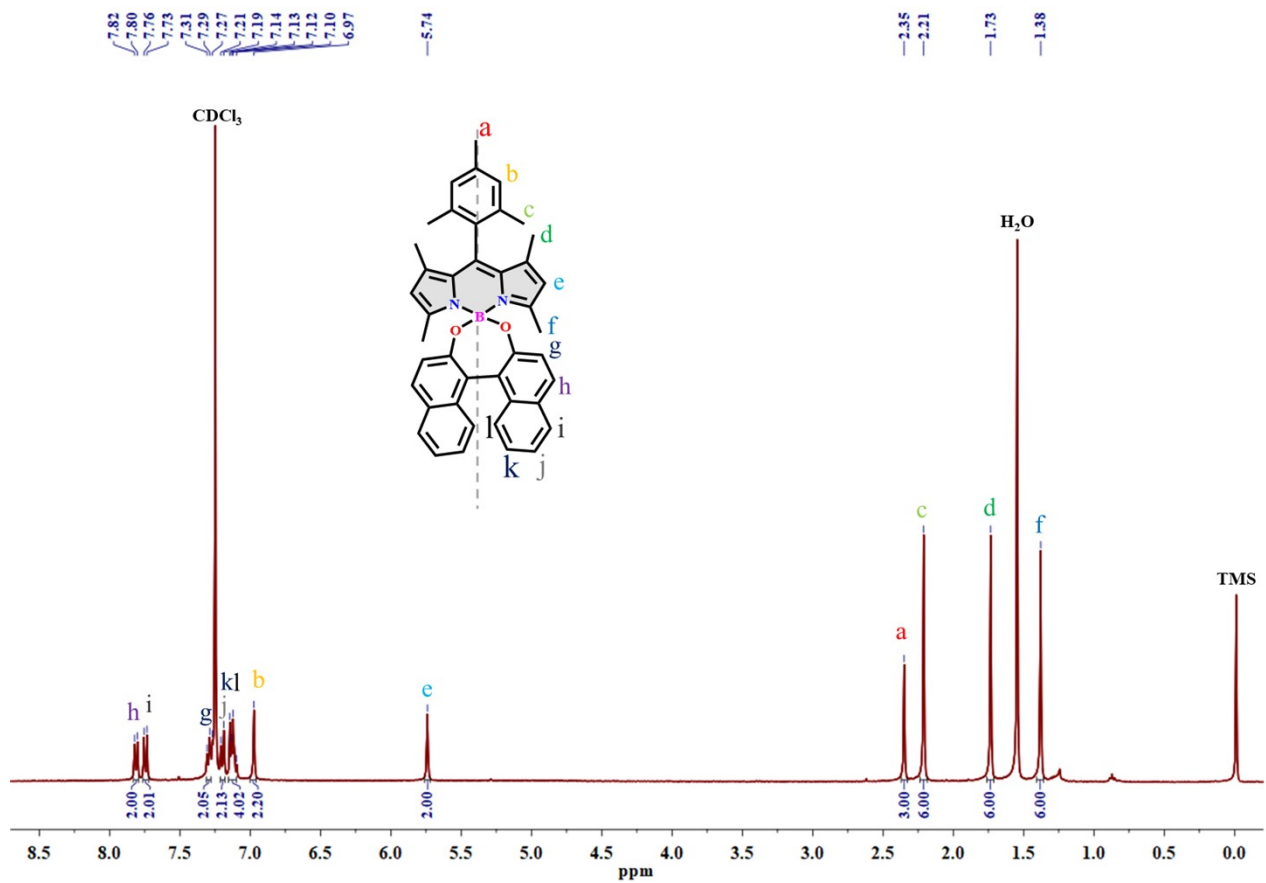


Figure S13. ^1H NMR spectrum of compound **OBP2** in CDCl_3 (298 K).

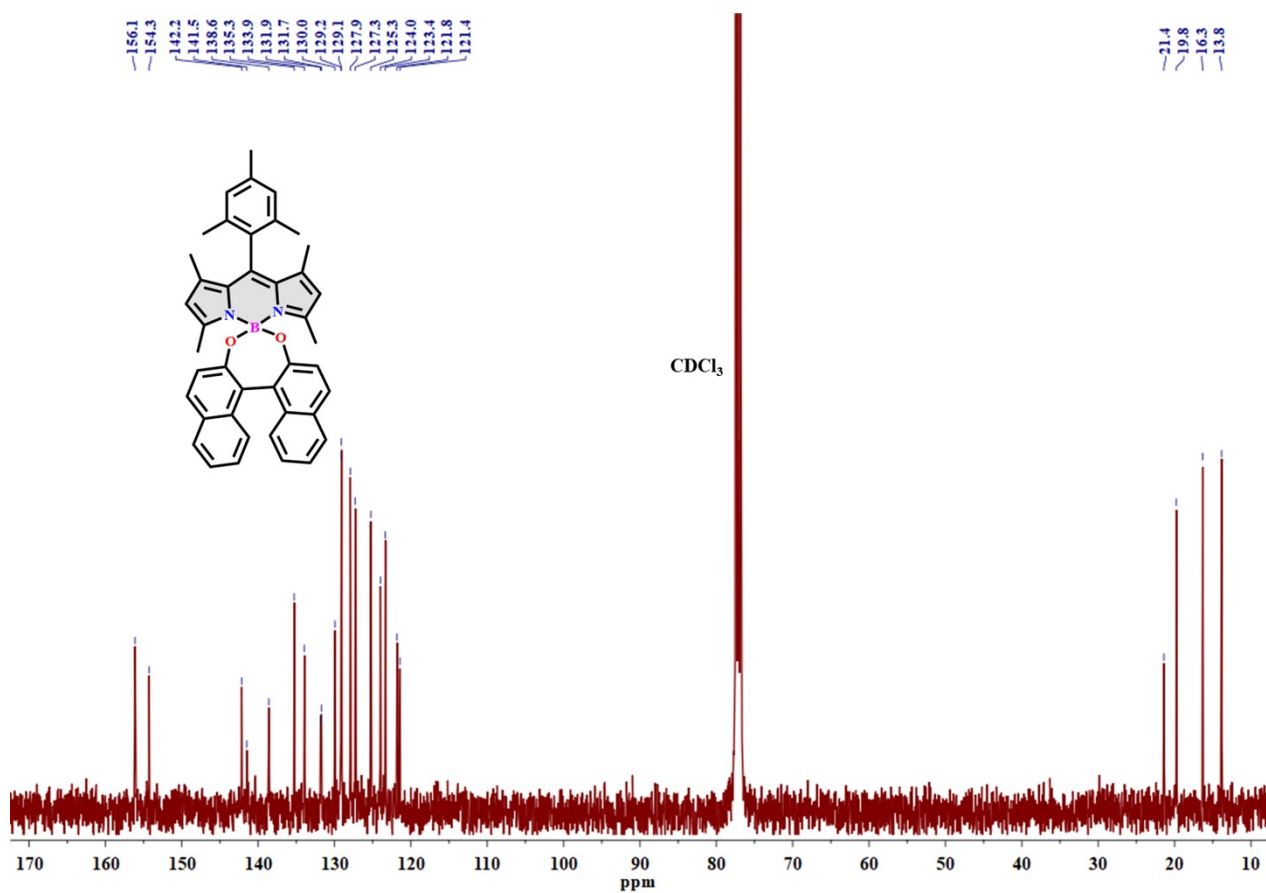


Figure S14. ^{13}C NMR spectrum of compound **OBP2** in CDCl_3 (298 K).

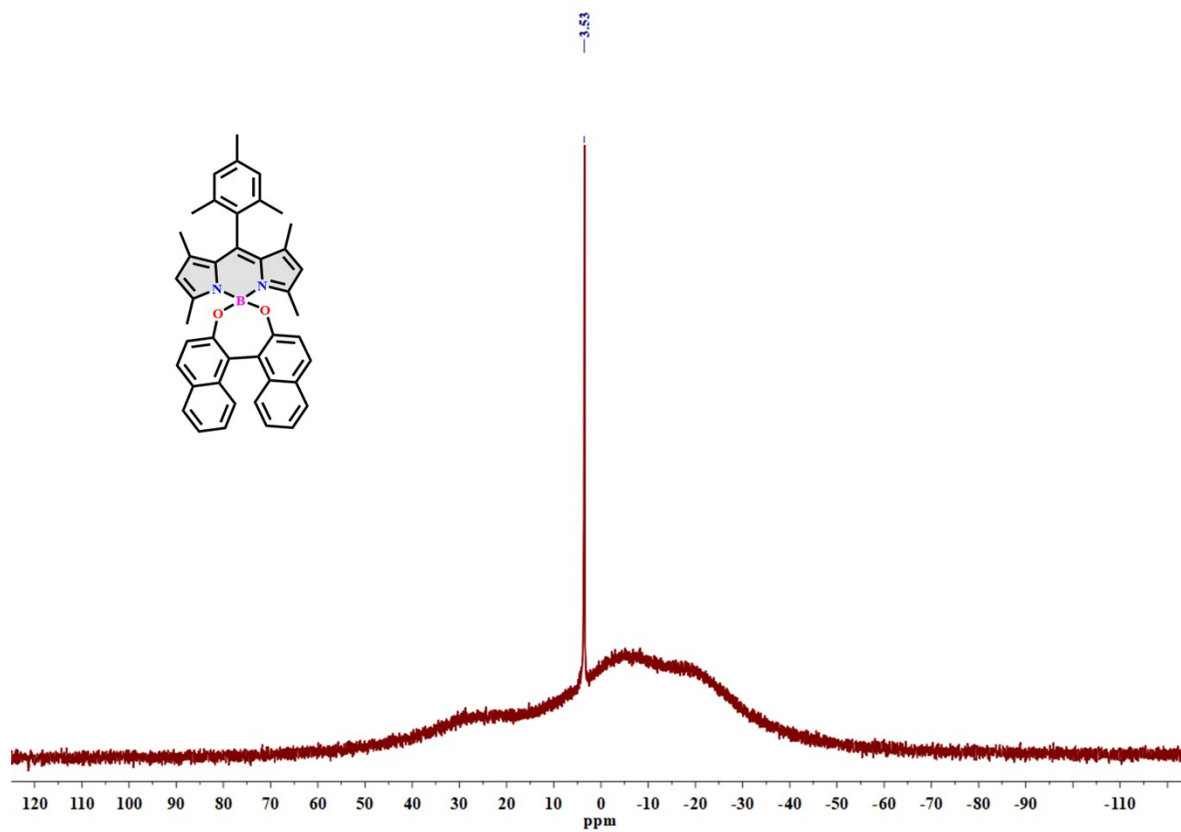


Figure S15. ^{11}B NMR spectrum of compound **OBP2** in CDCl_3 (298 K).

8. HRMS spectra of the spiranic 4,4-diaryloxy-BODIPY derivatives

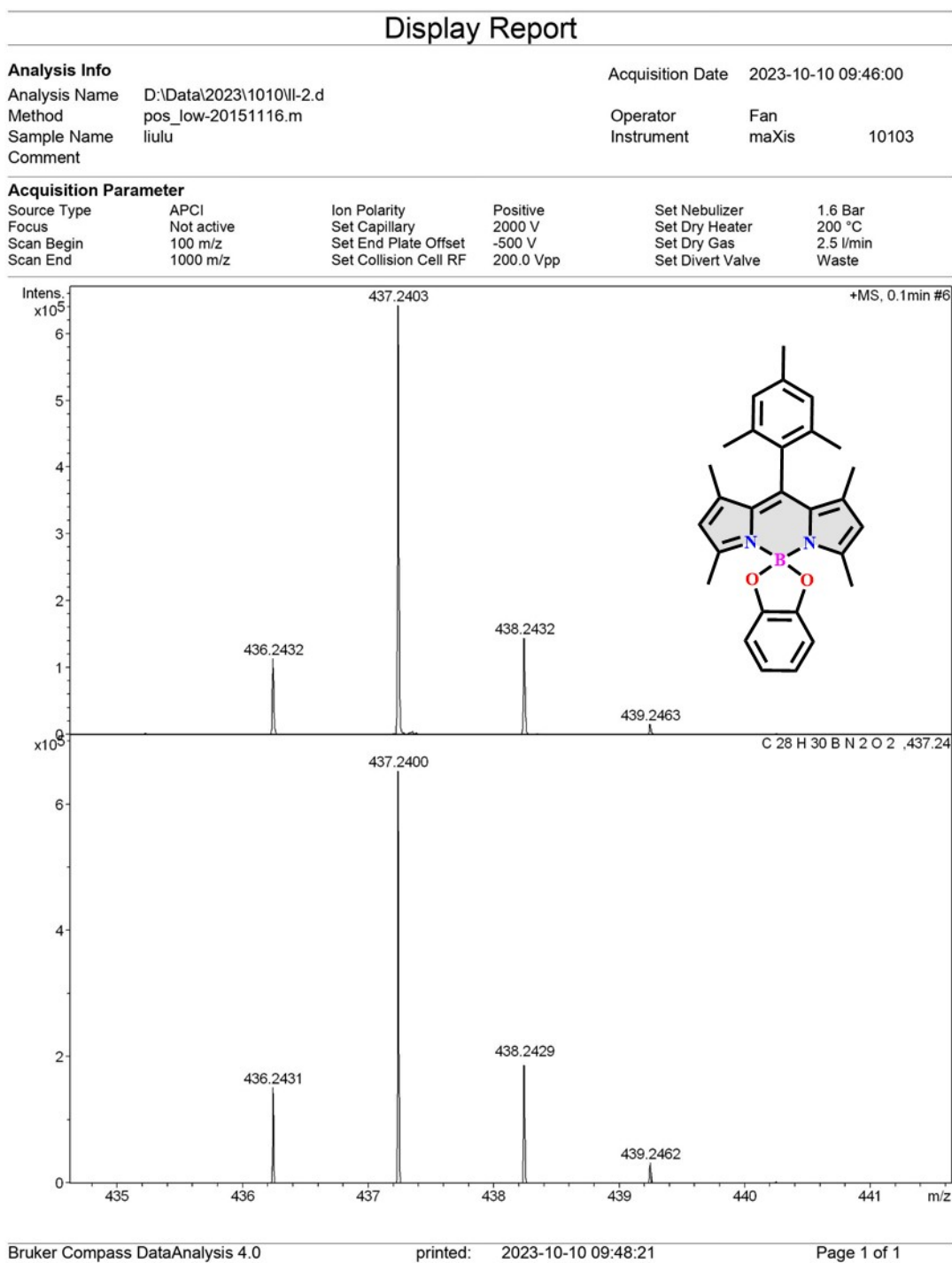


Figure S16. HRMS spectrum of compound **OBP1**.

Display Report

Analysis Info

Analysis Name D:\Data\2023\1010\II-4.d
Method pos_low-20151116.m
Sample Name liulu
Comment

Acquisition Date 2023-10-10 09:51:32
Operator Fan
Instrument maXis 10103

Acquisition Parameter

Source Type	APCI	Ion Polarity	Positive	Set Nebulizer	1.6 Bar
Focus	Not active	Set Capillary	2000 V	Set Dry Heater	200 °C
Scan Begin	100 m/z	Set End Plate Offset	-500 V	Set Dry Gas	2.5 l/min
Scan End	1000 m/z	Set Collision Cell RF	200.0 Vpp	Set Divert Valve	Waste

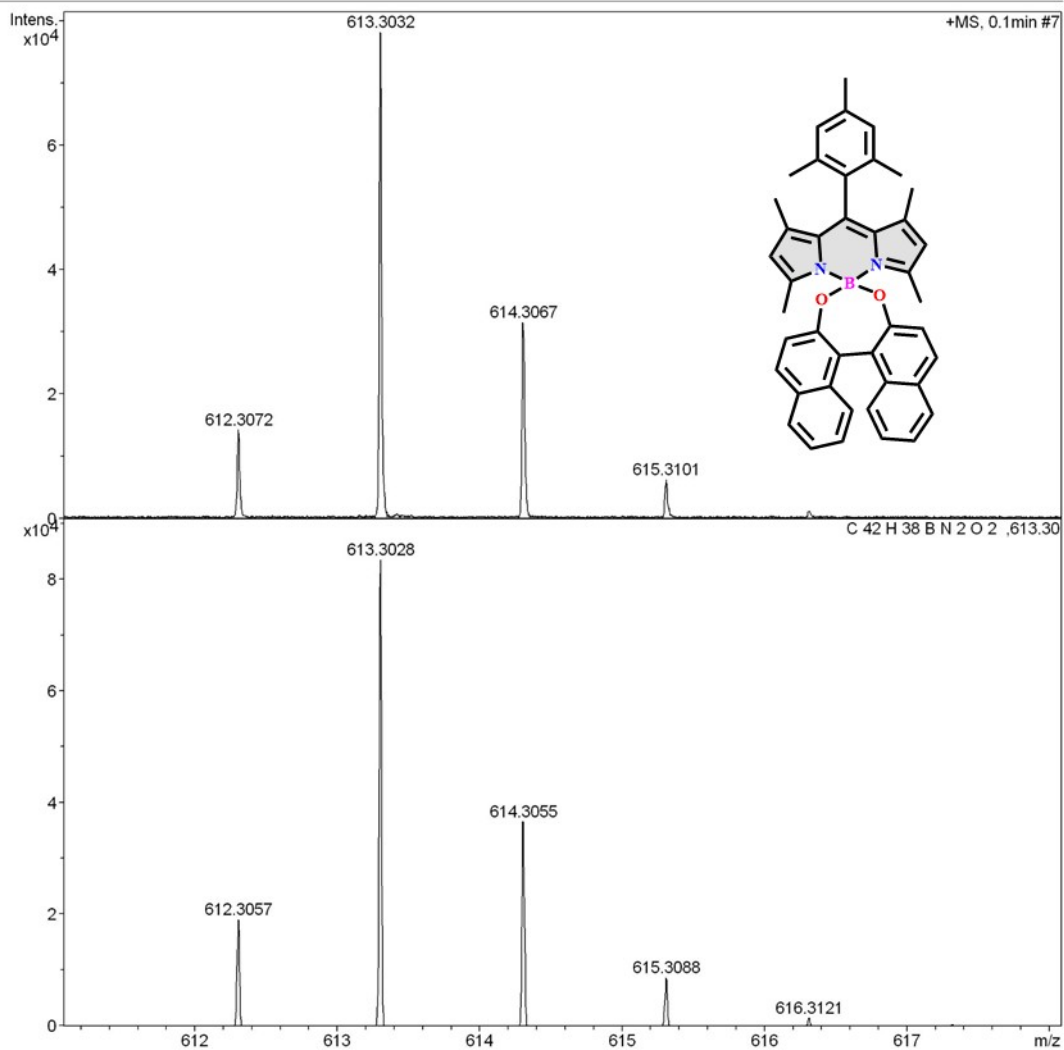


Figure S17. HRMS spectrum of compound OBP2.

References

- [1] E. M. Sánchez-Carnerero, F. Moreno, B. L. Maroto, A. R. Agarrabeitia, M. J. Ortiz, B. G. Vo, G. Muller, S. de la Moya. Circularly polarized luminescence by visible-light absorption in a chiral *O*-BODIPY dye: Unprecedented design of CPL organic molecules from achiral chromophores. *J. Am. Chem. Soc.* **2014**, *136*, 3346-3349.
- [2] S. Zhang, Y. Wang, F. Meng, C. Dai, Y. Cheng, C. Zhu. Circularly polarized luminescence of AIE-active chiral *O*-BODIPYs induced via intramolecular energy transfer. *Chem. Commun.* **2015**, *51* (43), 9014-9017.
- [3] L. Gartzia-Rivero, E. M. Sánchez-Carnerero, J. Jiménez, J. Bañuelos, F. Moreno, B. L. Maroto, I. López-Arbeloa, S. de la Moya. Modulation of ICT probability in bi(polyarene)-based *O*-BODIPYs: Towards the development of low-cost bright arene-BODIPY dyads. *Dalton Trans.* **2017**, *46* (35), 11830-11839.
- [4] H. A. A. El-Ali, J. Jing, X. Zhang. Solid-state emissive *O*-BODIPY dyes with bimodal emissions across red and near infrared region. *RSC Adv.* **2019**, *9* (28), 16246-16251.
- [5] Y. Sasaki, J. Gautier, M. Li, L. Karmazin, T. W. Ebbesen, C. Genet. Enhanced chiral exciton coupling in neat molecular films. *J. Phys. Chem. C.* **2023**, *127*, 18526-18532.
- [6] T. Liu, L. Ding, K. Zhao, W. Wang, Y. Fang. Single-layer assembly of pyrene end-capped terthiophene and its sensing performances to nitroaromatic explosives. *J. Mater. Chem.* **2012**, *22*, 1069-1077.
- [7] K. Liu, J. Zhang, Q. Shi, L. Ding, T. Liu, Y. Fang. Precise manipulation of excited-state intramolecular proton transfer via incorporating charge transfer toward high-performance film-based fluorescence sensing. *J. Am. Chem. Soc.* **2023**, *145* (13), 7408-7415.
- [8] J. Zhao, K. Liu, R. Wang, T. Liu, Z. Wu, L. Ding, Y. Fang. Dual-mode optical sensor array for detecting and identifying perillaldehyde in solution phase and plant leaf with smartphone. *ACS Appl. Mater. Interfaces* **2022**, *14* (47), 53323-53330.